PHOTONICS Research

Intermodal group-velocity engineering for broadband nonlinear optics

Jeff Demas,[1,2] Lars Rishøj,[1] Xiao Liu,[1] Gautam Prabhakar,[1] and Siddharth Ramachandran[1,*]

[1]Department of Electrical Engineering, Boston University, Boston, Massachusetts 02115, USA
[2]Currently with The Rockefeller University, New York, New York 10065, USA
*Corresponding author: sidr@bu.edu

Interest in the nonlinear properties of multi-mode optical waveguides has seen a recent resurgence on account of the large dimensionality afforded by the platform. The large volume of modes in these waveguides provides a new spatial degree of freedom for phase matching nonlinear optical processes. However, this spatial dimension is quantized, which narrows the conversion bandwidths of intermodal processes and constrains spectral and temporal tailoring of the light. Here we show that by engineering the relative group velocity within the spatial dimension, we can tailor the phase-matching bandwidth of intermodal parametric nonlinearities. We demonstrate group-velocity-tailored parametric nonlinear mixing between higher-order modes in a multi-mode fiber with gain bandwidths that are more than an order of magnitude larger than that previously thought possible for intermodal four-wave mixing. As evidence of the technological utility of this methodology, we seed this process to generate the first high-peak-power wavelength-tunable all-fiber quasi-CW laser in the Ti:sapphire wavelength regime. More generally, with the combination of intermodal interactions, which dramatically expand the phase-matching degrees of freedom for nonlinear optics, and intermodal group-velocity engineering, which enables tailoring of the bandwidth of such interactions, we showcase a platform for nonlinear optics that can be broadband while being wavelength agnostic.   © 2018 Chinese Laser Press

https://doi.org/10.1364/PRJ.7.000001

1. INTRODUCTION

Multi-mode optical fibers provide the ability to guide light while encoding spatial—in addition to traditional temporal and spectral—information. Recently, there has been renewed interest in using this spatial dimension for applications including imaging [1], high-capacity telecommunications [2,3], and high-power laser development [4,5]. Likewise, interest in their nonlinear optical properties has also grown, leading to many demonstrations of intermodal supercontinuum generation [6–8] and other ultrafast nonlinear phenomena [9–11]. Parametric processes that resonantly convert pump light directly to target frequency bands, for instance four-wave mixing (FWM), may especially benefit from the large dimensionality of multi-mode systems, as intermodal interactions drastically increase the number of possible combinations with which phase matching is achieved. This increased flexibility is being explored for applications such as optical signal processing [12,13], frequency conversion [14], and quantum entanglement [15,16].

There is one main difficulty in harnessing the multi-mode space, however. As illustrated in the first demonstration of intermodal nonlinear optics by Stolen *et al.* in 1974

[17,18]—and repeatedly confirmed by subsequent experimental investigations to date [19–23]—FWM between different spatial modes typically exhibits impractically narrow parametric gain bandwidths. This problem arises because transverse space in an optical fiber is discretized into modes rather than being continuous; thus, the modes have discrete phase velocities, and accordingly only discrete (i.e., narrowband) phase-matched combinations are typically found. Thus, the spatial degree of freedom is gained while constraining the two other crucial degrees of freedom related to spectral and temporal tailoring of light. This obviates the utility of intermodal interactions for most known applications of parametric nonlinear processes, such as multicasting classical communications signals [24], tailoring joint-spectral amplitudes for quantum sources [25], or ultrashort-pulse nonlinear interactions, to name a few examples.

Here, we demonstrate a solution to this problem by tailoring not only the phase-matching condition but also the relative group velocities of interacting modes in a multi-mode optical fiber. By matching the group velocity of the $LP_{0,4}$ and $LP_{0,5}$ modes [Fig. 1(a)] at their respective converted wavelengths, we upend conventional wisdom that intermodal FWM is
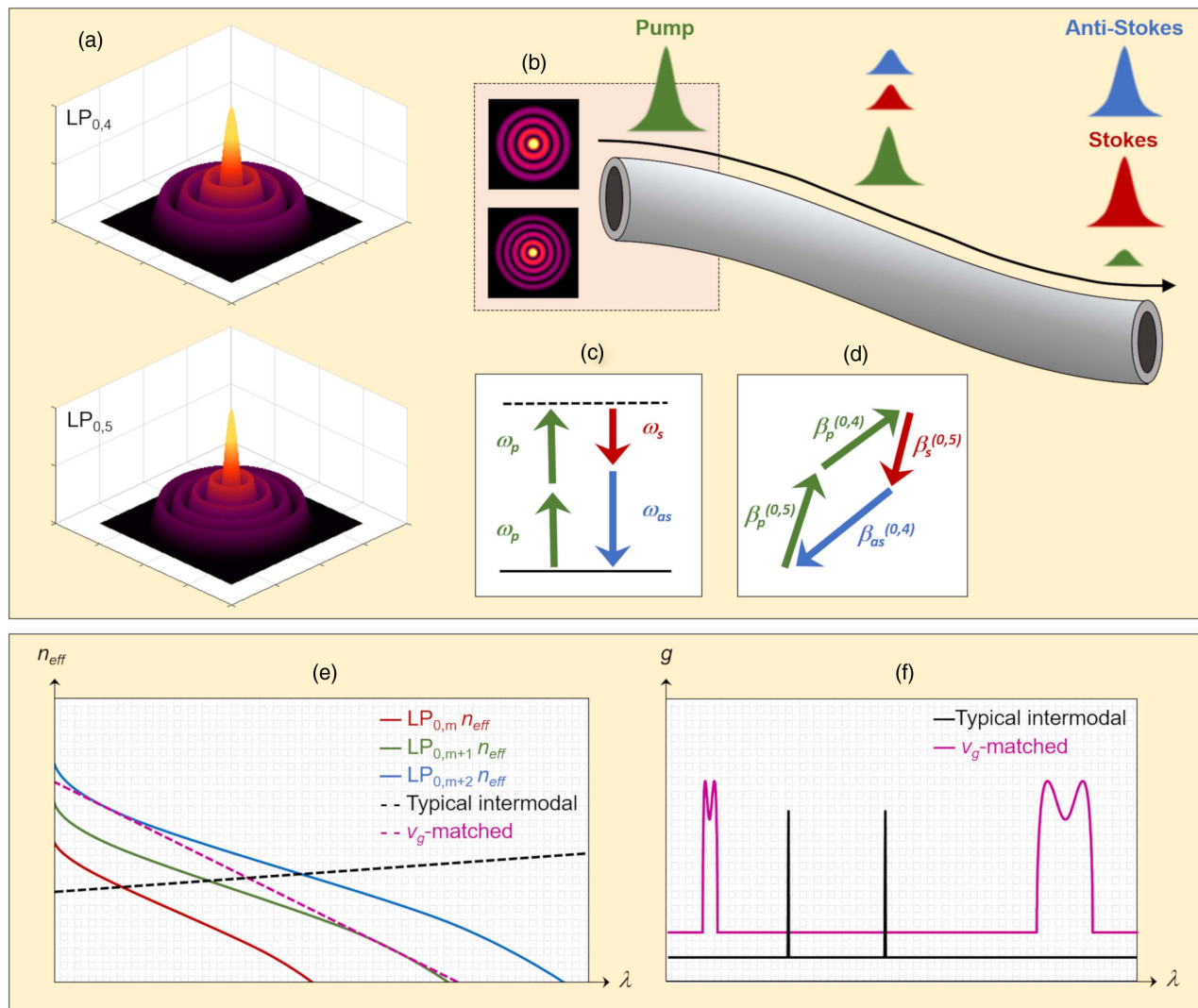
Fig. 1. (a) Intensity profiles of the pump modes $LP_{0,4}$ and $LP_{0,5}$. (b) Schematic representation of intermodal parametric frequency conversion of the pump (green pulse) to the anti-Stokes (blue pulse) and Stokes (red pulse) waves along the length of the fiber. Schematic representation of (c) energy conservation and (d) phase matching for four-wave mixing. (e) Phase matching in the effective refractive index picture: solutions exist where the straight, dashed lines intersect the n_{eff} curves for different modes (solid lines), where integer "m" denotes radial mode order. (f) Parametric gain for typical intermodal processes (black line) and a group-velocity-tailored process (purple line), offset for clarity; the purple line in (e) is tangent to the n_{eff} curves for an extended wavelength range leading to broadband parametric gain.

necessarily narrowband, and report, to the best of our knowledge, the first realization of broadband intermodal parametric frequency conversion (63 nm at 1553 nm, 17 nm at 791 nm). Additionally, we seed this process [Fig. 1(b)] to generate a high-peak-power (~10 kW) quasi-CW (~0.6 ns) source of wavelength-tunable radiation in the Ti:sapphire wavelength band (786–795 nm). Thus, group-velocity-matched intermodal FWM unlocks a degree of freedom that decouples interaction wavelengths from their respective bandwidths, while also providing for a power-scalable platform to achieve nonlinear frequency conversion.

2. INTERMODAL PHASE MATCHING

FWM (Fig. 1) requires that the energy of the photons (proportional to their respective frequencies) and their momenta

(proportional to the propagation constant β) be conserved [Figs. 1(c) and 1(d), pump is denoted by "p," Stokes by "s," and anti-Stokes by "as"]. The parameter β is related to the effective refractive index n_{eff}, by $\beta = 2\pi n_{eff}/\lambda$, and thus the phase-matching condition for FWM is given by

$$\Delta\beta = \frac{2\pi}{\lambda_p} n_{\text{eff}}^{(j)}(\lambda_p) + \frac{2\pi}{\lambda_p} n_{\text{eff}}^{(k)}(\lambda_p) - \frac{2\pi}{\lambda_s} n_{\text{eff}}^{(l)}(\lambda_s) - \frac{2\pi}{\lambda_{as}} n_{\text{eff}}^{(m)}(\lambda_{as}) \approx 0,$$

$$(1)$$

where λ is the wavelength; the super-scripts "j" through "m" correspond to the modes of each component of the pump, the Stokes field, and the anti-Stokes field, respectively; and the small offset due to self-phase modulation has been neglected [26]. It can be shown that for cases where the n_{eff} of all four fields lies on a straight line (when plotted versus wavelength) at

corresponding wavelengths that conserve energy, the waves are necessarily phase-matched (see the derivation in Supplement 1, section S.4 of Ref. [22]). This concept is illustrated in Fig. 1(e), which shows two exemplary phase-matching possibilities. The black dashed line corresponds to a typical intermodal case where two wavelength- and mode-degenerate pump photons couple to anti-Stokes and Stokes photons in adjacent mode orders. The line intersects the n_{eff} curves of the anti-Stokes, pump, and Stokes modes (solid red, green, and blue lines, respectively), leading to phase matching. Here we see the utility of the multi-mode space, in that more modes provide more avenues for phase matching. However, the slope of the phase-matching line is such that intersection points occur only for discrete sets of wavelengths, and thus the resulting parametric gain [black line in Fig. 1(f)] is intrinsically narrowband.

The purple dashed line in Fig. 1(e) depicts the n_{eff} phase-matching picture for a group-velocity-tailored intermodal process. The pump laser is equally partitioned between two modes, and thus the phase-matching line lies between their respective n_{eff} curves [solid blue and green lines in Fig. 1(e)] at the pump wavelength. By adjusting the pump wavelength, we can precisely energy-match the pump to the anti-Stokes and Stokes wavelengths such that the n_{eff} curves of the respective interacting modes are tangential to the phase-matching line. This condition is equivalent to the two modes being group-index-matched, and thus group-velocity-matched, at their respective anti-Stokes and Stokes wavelengths, and automatically yields broad gain bandwidths [purple line, Fig. 1(f)].

To explicitly derive the relationship between group velocity and bandwidth, we start by assuming the waves are phase- and energy-matched for a given set of frequencies such that $\Delta\beta = \beta_j(\omega_p) + \beta_k(\omega_p) - \beta_j(\omega_s) - \beta_k(\omega_{as}) = 0$ [where "j" and "k" are the indices of the two interacting modes, and $\beta = \omega n_{eff}(\omega)/c$]. To determine bandwidth, we assess phase matching for a small frequency detuning $\Delta\omega$ of the anti-Stokes and Stokes waves from the nominally phase-matched condition (note that the detuning is opposite in sign for the Stokes and anti-Stokes waves in order to conserve energy). We expand to the first order to approximate the frequency dependence [20,21],

$$\Delta\beta = \beta_j(\omega_p) + \beta_k(\omega_p) - \left[\beta_j(\omega_{as}) + \Delta\omega\frac{d\beta_j}{d\omega}\bigg|_{\omega_{as}}\right]$$
$$- \left[\beta_k(\omega_s) - \Delta\omega\frac{d\beta_k}{d\omega}\bigg|_{\omega_s}\right]. \qquad (2)$$

The zeroth-order terms cancel as the waves are nominally phase-matched, yielding

$$\Delta\beta = \Delta\omega\left(\frac{d\beta_k}{d\omega}\bigg|_{\omega_s} - \frac{d\beta_j}{d\omega}\bigg|_{\omega_{as}}\right). \qquad (3)$$

For the case where the derivatives of β for modes "j" and "k" evaluated at ω_{as} and ω_s are equal, the modes are phase matched (i.e., $\Delta\beta = 0$) for arbitrary bandwidth (higher-order terms are required to accurately predict the bandwidth). Group velocity is given by $v_g = (d\beta/d\omega)^{-1}$; therefore, matching the group velocities of the Stokes and anti-Stokes modes at their respective frequencies (wavelengths) maximizes the phase-matched bandwidth.

Phase matching in single-mode fibers (SMFs) can also be similarly graphically analyzed and serves to illustrate the unique design space enabled by the group-velocity-tailored intermodal FWM we discuss here. For SMFs, the availability of only one curve [Fig. 1(e)] implies that phase-matching wavelengths as well as bandwidths need to be controlled only by tailoring this single curve. Such tailoring, also called group-velocity-dispersion engineering, has been revolutionized with the advent of photonic crystal designs [27], but restricts the design freedom to two canonical parametric gain profiles: (1) broadband gain at wavelengths adjacent to the pump laser or (2) narrowband gain at wavelengths far from the pump [28–30]. In contrast, the group-velocity-tailored intermodal FWM platform we describe here faces no such bandwidth-versus-wavelength constraints.

3. EXPERIMENT AND RESULTS

Light from a home-built pulsed ytterbium-doped fiber laser ($\lambda = 1040$–1050 nm, $\tau = 1$ ns, 5 kHz repetition rate, ~ 70 kW peak power) is coupled into a 2 m segment of step-index multi-mode test fiber (50 μm core diameter, numerical aperture NA = 0.22, Thorlabs FG050LGA). We simulate the electric fields, effective indices, group velocities, and dispersion of the modes in the test fiber using a home-built scalar eigenmode solver operating on a measurement of the fiber's refractive index profile. We excite pump modes in the fiber using a binary phase plate programmed on a spatial light modulator [Fig. 2(a), Hamamatsu X10468] [31,32]. The phase plate is designed to match the phase reversals of the $LP_{0,5}$ mode but stretched larger than the optimum size for pure $LP_{0,5}$ excitation, resulting in coupling to both the $LP_{0,4}$ and $LP_{0,5}$ modes [Fig. 2(b)]. To ensure equal coupling to the $LP_{0,4}$ and $LP_{0,5}$ modes, we experimentally optimize phase plate stretching by maximizing spontaneous parametric fluorescence at the anti-Stokes wavelength, finding an optimum stretching factor of 12%. Simulations of the overlap between the electric field of the beam immediately after the SLM and each mode of the test fiber indicate that $\sim 81\%$ of the power coupled to the fiber resides in an equal (within 1%) superposition of the target $LP_{0,4}$ and $LP_{0,5}$ modes [Fig. 2(c)] [31].

The wavelength of the pump is chosen such that the group velocity [Fig. 2(d)] of the $LP_{0,4}$ mode at the anti-Stokes wavelength (7XX nm) is matched to that of the $LP_{0,5}$ mode at the Stokes wavelength (15XX nm). The corresponding simulated parametric gain curve shows broadband gain [Fig. 2(e)] centered at the group-velocity-matched wavelengths.

When only the pump laser is coupled into the fiber, the resultant spontaneous parametric fluorescence spectrum reveals the spectral dependence of the gain, and hence the phase-matched wavelengths and bandwidths. Figure 3(a) shows the measured parametric gain as a function of pump wavelength. Initially, there are two sets of gain peaks on the anti-Stokes and Stokes sides of the pump, respectively (purple curve, $\lambda = 1046.2$ nm). As the pump wavelength increases, the peaks move together and merge, and subsequently the gain decreases. This can be understood with the intuition provided by Fig. 1(e). Small changes in the pump wavelength change the energy-matching requirements, and accordingly change the
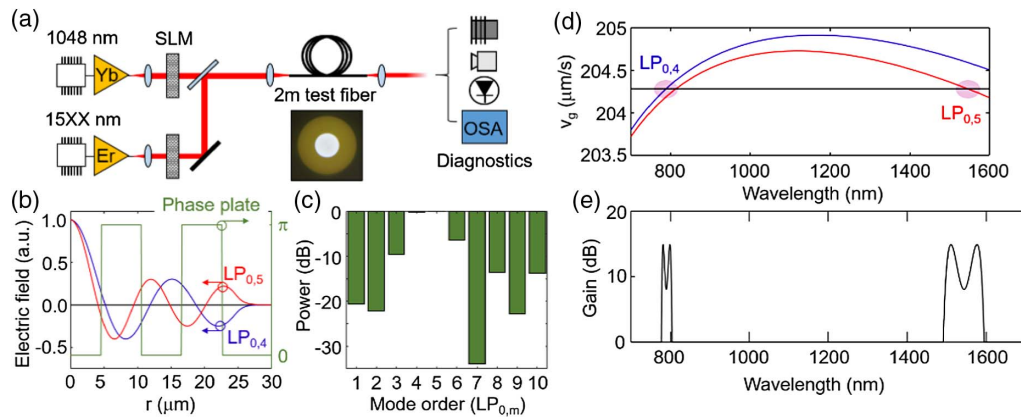
Fig. 2. (a) Setup schematic for intermodal four-wave mixing experiments. SLM, spatial light modulator; OSA, optical spectrum analyzer. (b) Simulated electric field profiles of the $LP_{0,4}$ (blue line) and $LP_{0,5}$ (red line) modes plotted alongside the phase profile of a $LP_{0,5}$ binary phase plate stretched by ~12% (green line, right axis). (c) Simulations of the relative power coupled to each mode of the test fiber for a phase plate stretched by 12%. (d) Simulated group velocity for the $LP_{0,4}$ and $LP_{0,5}$ modes. (e) Simulated parametric gain for group-velocity-matched four-wave mixing pumped with $LP_{0,4}$ and $LP_{0,5}$.

slope of the phase-matching line. For short pump wavelengths, the slope is larger and the line intersects the n_{eff} curves twice on either side of the pump, resulting in two sets of gain peaks. At longer pump wavelengths, the slope decreases, lying tangent to the n_{eff} curves and merging the gain peaks into one broadband region. If the slope decreases further, it no longer intersects the curves; phase matching is not preserved, and thus the gain disappears.

In order to maximize bandwidth, we operate at a pump wavelength of 1047.6 nm, where the line is slightly above the tangent point [see Fig. 1(e) for reference]. The two gain peaks have not completely merged, resulting in the characteristic dip in the center of the gain bandwidth. The measured gain [Fig. 3(b)] exhibits broadband regions (10 dB bandwidths of 63 nm at 1553 nm and 17 nm at 791 nm) in agreement with the simulations [Fig. 2(e)]. The measured image of the beam at the pump wavelength [inset in Fig. 3(b)] does not resemble the profile of a single $LP_{0,m}$ mode and exhibits rings with poor visibility, a hallmark of the intended superposition of modes. In contrast, the measured mode images at the anti-Stokes and Stokes wavelengths [inset in Fig. 3(b)] clearly correspond to the $LP_{0,4}$ and $LP_{0,5}$ modes, indicating wavelength conversion from the desired FWM process.

Next we introduce a low-power erbium-doped fiber laser coupled into the $LP_{0,5}$ mode of the test fiber and tune its wavelength across the Stokes gain band (15XX nm) [33]. This laser seeds the FWM process, causing transfer of power from the pump to the Stokes and anti-Stokes waves. Figure 4 shows measured output spectra for the system as a function of seed wavelength, indicating conversion of 1048 nm pump photons to the Ti:sapphire spectral region (786–795 nm) while maintaining the narrow spectral linewidth of the seed laser. Temporal profiles of the output pulses are shown in Figs. 5(a)–5(c). The center of the pump pulse undergoes depletion in the presence of the seed as the power is converted to the Stokes and anti-Stokes wavelengths [Fig. 5(a)]. In total, $34\% \pm 3\%$ of the pump power is depleted, with further depletion limited by the leading and trailing edges of the pump pulse, whose intensity is

not sufficient to drive the nonlinear process (as is commonly observed in any nonlinear process with pump pulses that are not temporally rectangular in shape). As a result, the output pulse widths for the Stokes and anti-Stokes pulses are narrowed to ~0.6 ns full width at half-maximum [Figs. 5(b) and 5(c)]. The conversion efficiency is $21\% \pm 2\%$ for the anti-Stokes wave and $10\% \pm 2\%$ for the Stokes wave. The discrepancy between the conversion efficiencies is because FWM preserves the photon number. Thus, the anti-Stokes photons, which are roughly twice as energetic as the Stokes photons, constitute the majority of the output power. Normalizing for photon energy,
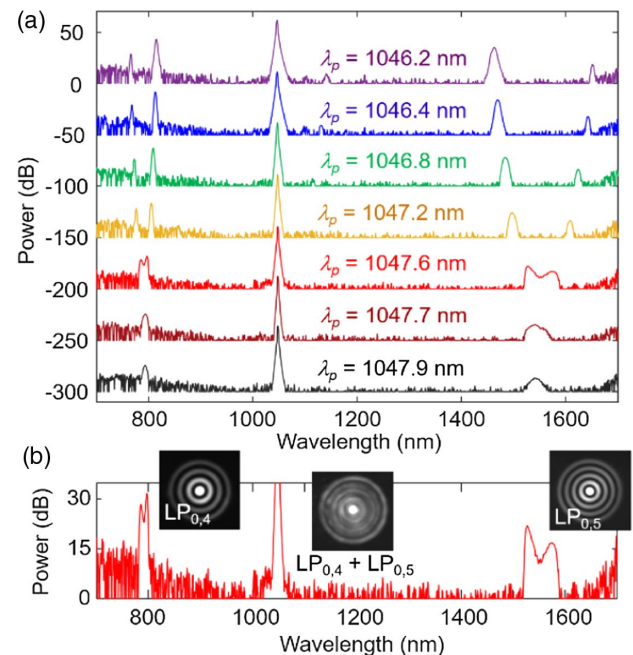

Fig. 3. (a) Spontaneous four-wave mixing spectra as a function of pump wavelength; each spectrum offset by 50 dB for clarity. (b) Zoom-in of the bandwidth-optimized spontaneous spectrum ($\lambda_p = 1047.6$ nm) with mode images inset.
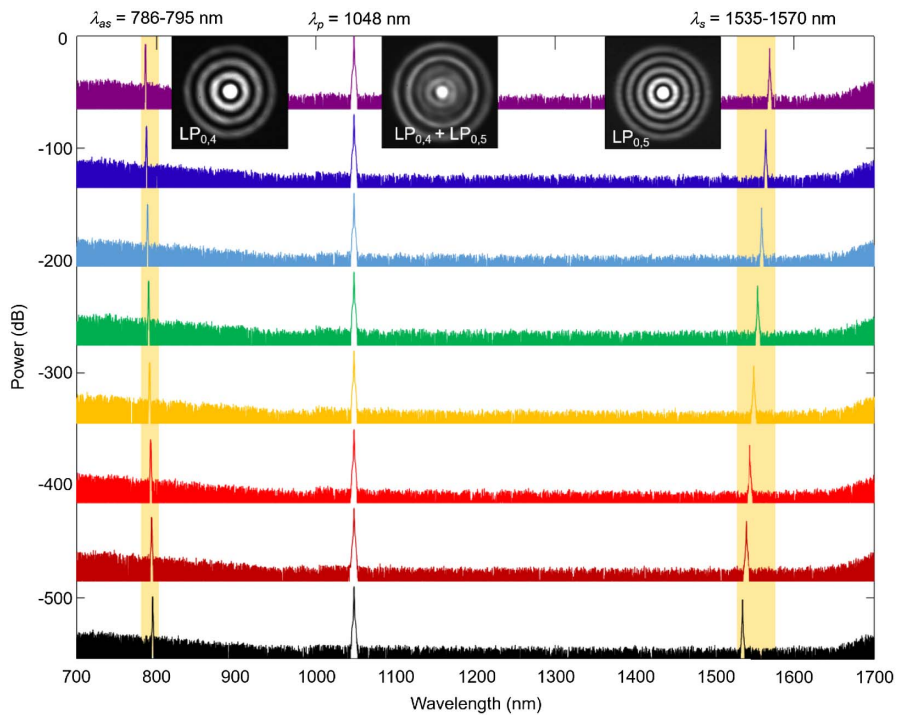
Fig. 4. Full experimental spectra as a function of seed wavelength (1535–1570 nm) showing conversion to the Ti:sapphire band (786–795 nm) with representative experimental mode images shown as inset; each spectrum offset by 70 dB for clarity.

the photon-to-photon transfer efficiencies from the pump to the anti-Stokes and Stokes wavelengths are in agreement (16% ± 2% and 15% ± 2%, respectively), as expected.

While the conversion efficiency is somewhat limited by the leading and trailing edges, the instantaneous depletion at the center of the pump pulse is as high as 71% [purple markers in Fig. 5(d)]. Efficient conversion of the peak of the pump pulse results in high peak powers of 11.2 kW for the anti-Stokes pulse [Fig. 5(b)] and 6 kW for the Stokes pulse [Fig. 5(c)], corresponding to ~48 dB of peak parametric gain at the seed

wavelength [brown markers in Fig. 5(d)]. Instantaneous pump depletion remains high across the full seed tuning range [purple markers in Fig. 5(d)], resulting in ~10 kW peak-power quasi-CW operation for all measured anti-Stokes pulses [Fig. 5(e)]. At the edges of the tuning range, we see no significant degradation of the system performance [Figs. 5(d) and 5(e)], implying that operation across the full ~17 nm bandwidth predicted by the spontaneous parametric fluorescence [Fig. 3(b)] would have been possible had we not been limited by the tunability of the seed source available in the laboratory.
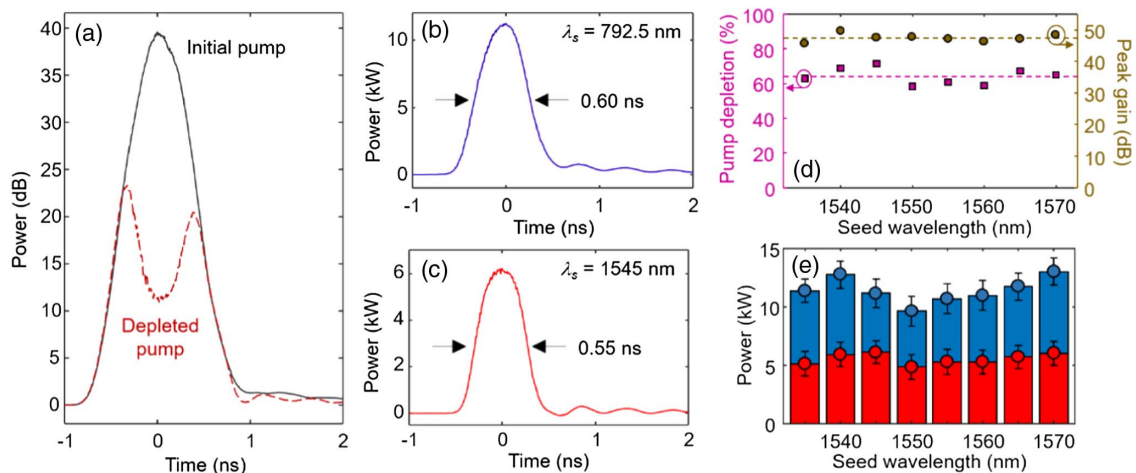

Fig. 5. Experimentally measured pump profiles for the (a) pump (pump alone shown as a solid black line; pump combined with seed shown as a dotted purple line), (b) anti-Stokes, and (c) Stokes wavelengths for a 1545 nm wavelength seed. (d) Peak pump depletion (purple markers, left axis) and peak Stokes gain (brown markers, right axis) as a function of seed wavelength. (e) Peak power (anti-Stokes shown with blue markers; Stokes shown with red markers).

Table 1. Additional Simulated Broadband FWM Processes

Pump Modes	Pump Wavelength	Stokes Bandwidth	Anti-Stokes Bandwidth
$LP_{0,1} + LP_{0,2}$	1194 nm	1519–1624 nm	943–984 nm
$LP_{0,2} + LP_{0,3}$	1142 nm	1548–1644 nm	874–904 nm
$LP_{0,3} + LP_{0,4}$	1093 nm	1533–1623 nm	823–849 nm
$LP_{0,4} + LP_{0,5}$[a]	1048 nm	1502–1586 nm	779–801 nm
$LP_{0,5} + LP_{0,6}$	1001 nm	1469–1552 nm	739–759 nm

[a]Corresponds to simulations of the experiments shown here.

To the best of our knowledge, these results represent the first demonstration of an ~10 kW peak-power wavelength-tunable fiber source operating in the 7XX nm wavelength regime. Additionally, the bandwidth supported by this system would enable conversion of pulses as short as ~40 fs. Hence, this represents the first all-fiber alternative to the ubiquitous Ti:sapphire laser that is the mainstay of many optics and photonics applications today.

4. DISCUSSION, SUMMARY, AND CONCLUSIONS

We have shown that by employing group-velocity matching between the $LP_{0,4}$ and $LP_{0,5}$ modes of a multi-mode fiber, we can overturn the decades-old conception that intermodal parametric interactions must be impractically narrowband and demonstrate a system that is wideband as well as broadband—a combination not afforded by single-mode nonlinear guided waves. This is possible because, unlike single-mode waveguides, in systems with spatial diversity, phase matching (related to the propagation constant of light) is decoupled from bandwidth (related to the spectral gradient of the propagation). Indeed, the ubiquity of this concept is not restricted to the specific mode combinations we used in our experiments. Rather, as Table 1 illustrates, other processes with similar spectral and modal degeneracies can result in a wide variety of spectral ranges in which broadband intermodal nonlinear interactions can be obtained, simply by choice of mode order. More generally, we expect this phenomenon to hold true for modes with entirely different symmetries, and waveguide design may enable group-velocity-matched parametric nonlinearities in platforms other than fibers, such as on-chip waveguides.

Technologically, employing group-velocity engineering to multi-mode nonlinear optics reveals two benefits: (1) by enabling bandwidth tailoring independent of phase-matching constraints, it facilitates control over the spectral distribution of the nonlinear response agnostic of the wavelength of operation, thereby addressing applications such as multi-mode multicasting and factorable or non-factorable quantum state generation, and (2) by decoupling the phase-matching condition and bandwidth from mode area, tunable frequency-converted sources become power scalable in an all-fiber schematic. As such, intermodal group-velocity engineering promises advances in controlling, exploiting, or managing optical nonlinearities in multi-mode optical systems, in analogy to the revolutionary advances in single-mode nonlinear optics made possible by dispersion engineering afforded by photonic crystal designs.

REFERENCES

1. T. Čižmár and K. Dholakia, "Exploiting multimode waveguides for pure fibre-based imaging," Nat. Commun. **3**, 1027 (2012).
2. R. J. Essiambre, R. Ryf, N. K. Fontaine, and S. Randel, "Breakthroughs in photonics 2012: space-division multiplexing in multimode and multicore fibers for high-capacity optical communication," IEEE Photon. J. **5**, 0701307 (2013).
3. N. Bozinovic, Y. Yue, Y. Ren, M. Tur, P. Kristensen, H. Huang, A. E. Willner, and S. Ramachandran, "Terabit-scale orbital angular momentum mode division multiplexing in fibers," Science **340**, 1545–1548 (2013).
4. J. W. Nicholson, J. M. Fini, A. M. DeSantolo, X. Liu, K. Feder, P. S. Westbrook, V. R. Supradeepa, E. Monberg, F. DiMarcello, R. Ortiz, C. Headley, and D. J. DiGiovanni, "Scaling the effective area of higher-order-mode erbium-doped fiber amplifiers," Opt. Express **20**, 24575–24584 (2012).
5. S. Ramachandran, J. M. Fini, M. Mermelstein, J. W. Nicholson, S. Ghalmi, and M. F. Yan, "Ultra-large effective-area, higher-order mode fibers: a new strategy for high-power lasers," Laser Photon. Rev. **2**, 429–448 (2008).
6. B. Zwan, S. Legge, J. Holdsworth, and B. King, "Spatio-spectral analysis of supercontinuum generation in higher order electromagnetic modes of photonic crystal fiber," Opt. Express **21**, 834–839 (2013).
7. Y. Chen, Z. Chen, W. J. Wadsworth, and T. A. Birks, "Nonlinear optics in the LP_{02} higher-order mode of a fiber," Opt. Express **21**, 17786–17799 (2013).
8. S. O. Konorov, E. E. Serebrannikov, A. M. Zheltikov, P. Zhou, A. Tarasevitch, and D. von der Linde, "Mode-controlled colors from microstructure fibers," Opt. Express **12**, 730–735 (2004).
9. L. Rishøj, B. Tai, P. Kristensen, and S. Ramachandran, "Discovery of soliton self-mode conversion in multimode optical fibers," arXiv:1805.06037.
10. L. G. Wright, D. N. Christodoulides, and F. W. Wise, "Controllable spatiotemporal nonlinear effects in multimode fibres," Nat. Photonics **9**, 306–310 (2015).
11. K. Krupa, A. Tonello, B. M. Shalaby, M. Fabert, A. Barthélémy, G. Millot, S. Wabnitz, and V. Couderc, "Spatial beam self-cleaning in multimode fibres," Nat. Photonics **11**, 237–241 (2017).
12. M. Schnack, T. Hellwig, and K. Fallnich, "Ultrafast, all-optical control of modal phases in a few-mode fiber for all-optical switching," Opt. Lett. **41**, 5588–5591 (2016).
13. M. Ma and L. R. Chen, "Harnessing mode-selective nonlinear optics for on-chip multi-channel all-optical signal processing," APL Photon. **1**, 086104 (2016).
14. J. Demas, G. Prabhakar, T. He, and S. Ramachandran, "Wavelength-agile high-power sources via four-wave mixing in higher-order modes," Opt. Express **25**, 7455–7464 (2017).
15. D. Cruz-Delgado, R. Ramirez-Alarcon, E. Ortiz-Ricardo, J. Monroy-Ruz, F. Dominguez-Serna, H. Cruz-Ramirez, K. Garay-Palmett, and A. B. U'Ren, "Fiber-based photon-pair source capable of hybrid entanglement in frequency and transverse mode, controllably scalable to higher dimensions," Sci. Rep. **6**, 27377 (2016).
16. K. Rottwitt, J. G. Koefoed, and E. N. Christensen, "Photon-pair sources based on intermodal four-wave mixing in few-mode fibers," Fibers **6**, 32–34 (2018).
17. R. H. Stolen, J. E. Bjorkholm, and A. Ashkin, "Phase-matched three-wave mixing in silica fiber optical waveguides," Appl. Phys. Lett. **24**, 308–310 (1974).
18. R. H. Stolen, "Phase-matched-stimulated four-photon mixing in silica-fiber waveguides," IEEE J. Quantum Electron. **11**, 100–103 (1975).
19. J. Cheng, M. E. V. Pedersen, K. Charan, K. Wang, C. Xu, L. Grüner-Nielsen, and D. Jakobsen, "Intermodal four-wave mixing in a higher-order-mode fiber," Appl. Phys. Lett. **101**, 161106 (2012).
20. R. Essiambre, M. A. Mestre, R. Ryf, A. H. Gnauck, R. W. Tkach, A. R. Chraplyvy, Y. Sun, X. Jiang, and R. Lingle, "Experimental

investigation of inter-modal four-wave mixing in few-mode fibers," IEEE Photon. Technol. Lett. **25**, 539–542 (2013).

21. S. M. M. Friis, I. Begleris, Y. Jung, K. Rottwitt, P. Petropoulos, D. J. Richardson, P. Horak, and F. Parmigiani, "Inter-modal four-wave mixing study in a two-mode fiber," Opt. Express **24**, 30338–30348 (2016).

22. J. Demas, P. Steinvurzel, B. Tai, L. Rishøj, Y. Chen, and S. Ramachandran, "Intermodal nonlinear mixing with Bessel beams in optical fiber," Optica **2**, 14–17 (2015).

23. H. Pourbeyram, E. Nazemosadat, and A. Mafi, "Detailed investigation of intermodal four-wave mixing in SMF-28: blue-red generation from green," Opt. Express **23**, 14487–14500 (2015).

24. C.-S. Bres, A. O. J. Wiberg, B. P.-P. Kuo, N. Alic, and S. Radic, "Wavelength multicasting of 320-Gb/s channel in self-seeded parametric amplifier," IEEE Photon. Technol. Lett. **21**, 1002–1004 (2009).

25. B. Fang, O. Cohen, M. Liscidini, J. E. Sipe, and V. O. Lorenz, "Fast and highly resolved capture of the joint spectral density of photon pairs," Optica **1**, 281–284 (2014).

26. G. P. Agrawal, *Nonlinear Fiber Optics* (Elsevier, 2005).

27. J. C. Knight, J. Arriaga, T. A. Birks, A. Ortigosa-Blanch, W. J. Wadsworth, and P. St. J. Russell, "Anomalous dispersion in a photonic crystal fiber," IEEE Photon. Technol. Lett. **12**, 807–809 (2000).

28. D. Nodop, C. Jauregui, D. Schimpf, J. Limpert, and A. Tünnermann, "Efficient high-power generation of visible and mid-infrared light by degenerate four-wave-mixing in a large-mode-area photonic-crystal fiber," Opt. Lett. **34**, 3499–3501 (2009).

29. J. Hansryd, P. A. Andrekson, M. Westlund, J. Li, and P. O. Hedekvist, "Fiber-based optical parametric amplifiers and their applications," IEEE J. Sel. Top. Quantum Electron. **8**, 506–520 (2002).

30. P. Steinvurzel, J. Demas, B. Tai, Y. Chen, L. Yan, and S. Ramachandran, "Broadband parametric wavelength conversion at 1 μm with large mode area fibers," Opt. Lett. **39**, 743–746 (2014).

31. J. Demas, L. Rishøj, and S. Ramachandran, "Free-space beam shaping for precise control and conversion of modes in optical fiber," Opt. Express **23**, 28531–28545 (2015).

32. J. Demas, G. Prabhakar, T. He, and S. Ramachandran, "Broadband and Wideband parametric gain via intermodal four-wave mixing in optical fiber," in *Conference on Lasers and Electro-Optics (CLEO)* (2017), paper SM3M.1.

33. J. Demas, L. Rishøj, X. Liu, G. Prabhakar, and S. Ramachandran, "High-power, wavelength-tunable NIR all-fiber lasers via intermodal four-wave mixing," in *Conference on Lasers and Electro-Optics (CLEO)* (2017), paper JTh5A.8.